JACS
JOURNAL OF THE AMERICAN CHEMICAL SOCIETY
pubs.acs.org/JACS
Article

Photocatalysis of a Dinuclear Ru(II)−Re(I) Complex for CO_2 Reduction on a Solid Surface

Daiki Saito, Yasuomi Yamazaki, Yusuke Tamaki, and Osamu Ishitani*

Cite This: https://dx.doi.org/10.1021/jacs.0c09170
Read Online

ABSTRACT: The development of CO_2-reduction photocatalysts is one of the main targets in the field of artificial photosynthesis. Recently, numerous hybrid systems in which supramolecular photocatalysts comprised of a photosensitizer and catalytic-metal-complex units are immobilized on inorganic solid materials, such as semiconductors or mesoporous organosilica, have been reported as CO_2-reduction photocatalysts for various functions, including water oxidation and light harvesting. In the present study, we investigated the photocatalytic properties of supramolecular photocatalysts comprised of a Ru(II)-complex photosensitizer and a Re(I)-complex catalyst fixed on the surface of insulating Al_2O_3 particles: the distance among the supramolecular photocatalyst molecules should be fixed. Visible-light irradiation of the photocatalyst in the presence of an electron donor under a CO_2 atmosphere produced CO selectively. Although CO formation was also observed for a 1:1 mixture of mononuclear Ru(II) and Re(I) complexes attached to an Al_2O_3 surface, the photocatalytic activity was much lower. The activity of the Al_2O_3-supported photocatalyst was strongly dependent on the adsorption density of the supramolecular moiety, where the initial rate of photocatalytic CO formation was faster at lower density and higher photocatalyst durability was achieved at higher density. One of the main reasons for the former phenomenon is the decreased quenching fraction of the excited state of the photosensitizer unit by the reductant dissolved in the solution phase in the case of higher density. This is due to the self-quenching of the excited photosensitizer unit and steric hindrance between the condensed supramolecular photocatalyst molecules attached to the surface. The higher durability of the more condensed system is caused by intermolecular electron transfer between reduced supramolecular photocatalyst molecules, which accelerates the formation of CO in the photocatalytic CO_2 reduction. Coadsorption of a Ru(II) mononuclear complex as a redox photosensitizer could drastically reinforce the photocatalysis of the supramolecular photocatalyst on the surface of the Al_2O_3 particles: more than 10 times higher turnover number and about 3.4 times higher turnover frequency of CO formation. These investigations provide new architectures for the construction of efficient and durable hybrid photocatalytic systems for CO_2 reduction, which are composed of metal-complex photocatalysts and solid materials.

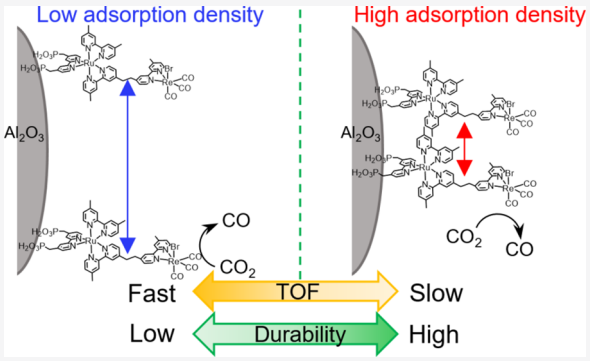

■ INTRODUCTION

Global warming and the depletion of fossil resources are serious threats to the future of human beings. Artificial photosynthesis in which CO_2 is converted to useful high-energy chemicals using solar light as the energy source is one of the most promising technologies for addressing both of these problems. However, various functionalities must be added to artificial photosynthesis systems if they are to be practically useful. In such systems, CO_2 must be photochemically reduced because it is a highly oxidized stable carbon compound. Photochemical electron transfer should be used for this purpose where, in principle, one-photon excitation induces only one-electron transfer. However, one-electron reduction of CO_2 requires very high energy (E_0 = −1.9 V vs NHE), and the product $CO_2^{-\bullet}$ is too active to be stored.[1,2] Conversely, multielectron reduction (typically two-electron reduction) of CO_2 drastically lowers the reduction potential of CO_2 and affords useful chemicals, e.g., CO and HCOOH, as two-electron-reduced compounds (eqs 1 and 2).[3]

Since some metal-complex catalysts can accept two electrons and introduce them to activated CO_2 to give CO and/or HCOOH,[4−9] various photocatalytic systems for CO_2 reduction have been constructed using such catalysts together with redox-photosensitizer metal complexes that initiate photochemical one-electron transfer from a reductant to the catalyst.[10−14] Recently, so-called supramolecular photocatalysts in which photosensitizer and catalysts units are connected have

Received: August 26, 2020

been widely researched owing to their superior photocatalytic abilities compared to those of the corresponding mixed systems in solution.[15−21] It has been reported that rapid intramolecular electron transfer from the reduced photosensitizer unit to the catalyst unit is a crucial process in the reduction of CO_2 in supramolecular photocatalytic systems.[22,23]

$$CO_2(g) + 2e^- + 2H^+ \rightarrow CO + H_2O \quad \overset{E_0/\mathrm{V\ vs\ NHE}}{-0.52\ \mathrm{V}} \tag{1}$$

$$CO_2(g) + 2e^- + 2H^+ \rightarrow HCOOH \quad -0.61\ \mathrm{V} \tag{2}$$

Although there are highly efficient photocatalytic systems for CO_2 reduction consisting of metal complexes alone,[10−14] these photocatalysts require a sacrificial electron donor to promote CO_2 reduction owing to their weak oxidation powers in the excited state. Furthermore, their light-absorption abilities are insufficient for the efficient use of solar light. Thus, in order to realize artificial photosynthesis for use in practical technologies, the addition of water oxidation and light-harvesting functions to such photocatalytic systems is necessary.

A useful strategy for the addition of such functions to metal-complex photocatalysts is the hybridization with functional solid materials.[24−32] Recently, supramolecular photocatalysts have been composited with various solid materials to fabricate hybrid photocatalysts.[33−37] The combination of supramolecular photocatalysts with semiconductors improves the photochemical oxidation power of such photocatalytic systems.[38] As a typical example, a photoelectrochemical cell consisting of a Ru(II)−Re(I) supramolecular photocatalyst fixed on a p-type semiconductor such as NiO and $CuGaO_2$ as a photocathode and an n-type semiconductor photoanode such as CoO_x/TaON can photocatalytically reduce CO_2 to CO using water as a reductant and visible light as energy.[39,40] Such high reduction and oxidizing powers are produced by stepwise excitation of the n-type semiconductor electrode and the Ru(II)-complex photosensitizer unit of the supramolecular photocatalyst. This is the so-called Z-scheme mechanism. A hybrid system comprised of a Ru(II)−Re(I) supramolecular photocatalyst fixed to the surface of periodic mesoporous organosilica (PMO), where the walls contained acridone molecules as light absorber units, has also been reported as a photocatalytic system with light-harvesting functionality.[41] In this system, photon energy absorbed by approximately 40 acridone units in the wall is efficiently transferred to one Ru(II) photosensitizer unit and initiates efficient photocatalytic CO_2 reduction.

In these hybrid systems containing solid materials, the supramolecular photocatalysts work much better than a mixed system of the corresponding mononuclear complexes. Although we may assume that one of the reasons for this is the rapid intramolecular electron transfer between the photosensitizer and catalyst units in the supramolecular photocatalyst, no systematic investigation into the superiority of supramolecular photocatalysts over the corresponding mixed systems on solid materials has been reported. There are several important mechanistic questions regarding CO_2 reduction using supramolecular photocatalysts, both on the surfaces of solid materials and in homogeneous solutions. One such question is how the catalyst unit can obtain the second electron. It has already been reported that the first reduction process proceeds via reductive quenching of the excited photosensitizer unit by a reductant followed by rapid intramolecular electron transfer from the reduced photosensitizer unit to the catalyst unit.[22,23,42,43] However, reduction of CO_2 to CO or HCOOH requires two electrons, as described above, but the photosensitizer unit can supply only one electron to the catalyst unit. Can a photosensitizer photochemically supply another electron to a catalyst unit that has already accepted one electron and reacted with CO_2? Does disproportionation of two reduced supramolecular photocatalyst molecules give "two-electron reduced" species upon their collision in homogeneous solution? Although the answers to these questions are important for developing more useful hybrid solid systems with metal-complex photocatalysts, the reported hybrid systems comprised of metal complexes and photofunctional solid materials promote their photocatalytic reactions via many and complicated processes, and this complexity makes it difficult to answer these questions.

Immobilization of the metal-complex photocatalysts onto nonphotoactive solid surfaces could provide a selective control method by introducing distance between the photosensitizer and the catalyst in mixed systems and also between the supramolecular photocatalyst molecules as well. In other words, changing the adsorption density of metal complexes with strong anchoring groups on insulators can systematically change surface distances. This could provide important information for answering the questions above.

Herein, a supramolecular photocatalyst consisting of a Ru(II) photosensitizer with methyl phosphonic acid groups as anchors and a Re(I) catalyst (**RuRe** in Chart 1) was adsorbed on Al_2O_3 insulator nanoparticles, and the effects of the adsorption density of **RuRe** on its photocatalytic ability for CO_2 reduction were investigated in detail. Photocatalytic CO_2 reduction was also conducted by using mononuclear **Ru** and **Re** complexes (Chart 1) immobilized on the Al_2O_3 together, and the results are compared with those using **RuRe**.

Chart 1. Structures and Abbreviations of the Metal Complexes Used in This Study

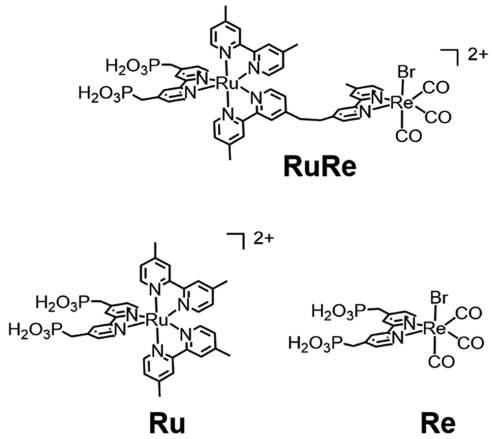

■ RESULTS AND DISCUSSION

The complexes **RuRe**, **Ru**, and **Re**, which each have a diimine ligand with two methylphosphonic acid anchor groups (Chart 1), were synthesized according to previous reports.[41,44,45] In this study, SiO_2 (AEROSIL OX 50) and Al_2O_3 (AEROXIDE Alu C) were used as solid insulators to adsorb the metal complexes on their surfaces because photochemical electron transfer between the complex and the solid material can be avoided. Since these solid particles, of which the average

https://dx.doi.org/10.1021/jacs.0c09170
J. Am. Chem. Soc. XXXX, XXX, XXX−XXX

particle sizes are 200−300 nm, are nonporous, the average distances between the metal complexes absorbed on the surface can be estimated from the surface area of the particles and the number of adsorbed metal complex molecules. Al_2O_3 or SiO_2 particles were added into an MeCN solution containing the metal complex or complexes, and the suspension was stirred under Ar atmosphere at room temperature for 7 days. The particles were collected by filtration and washed with MeCN several times until the filtrate did not contain the metal complex(es). The amount of the metal complex adsorbed was determined by measuring the amounts of the metal complex dissolved in the solution before and after the addition of the particles. We assessed the desorption of the complexes from the solid materials by the following method: The solid material adsorbing **RuRe** as described above (**RuRe**/Al_2O_3 and **RuRe**/SiO_2, the adsorption density: 5 μmol g^{-1}) was dispersed into a mixed solution of *N*,*N*-dimethylacetoamide (DMA)−triethanolamine (TEOA) (4:1, v/v) in the dark for 60 h, and then the solid was filtered. The UV−vis absorption spectrum of the filtrate was measured to determine the amount of **RuRe** desorbed from the solid material. In the case of **RuRe**/Al_2O_3, only 1% of the adsorbed **RuRe** was desorbed, while 12% was desorbed in the case of **RuRe**/SiO_2. Therefore, we chose Al_2O_3 particles as the solid material for all subsequent experiments. The amounts of the metal complex(es) adsorbed (AA) were obtained by using eq 3.

$$\mathrm{AA}\ (\mu\mathrm{mol\ g^{-1}}) = \frac{A_{\mathrm{before}} - A_{\mathrm{after}}}{A_{\mathrm{before}}} \times \frac{50\ [\mu\mathrm{M}] \times 50\ [\mathrm{mL}]}{X\ [\mathrm{mg}]} \tag{3}$$

where A_{before} and A_{after} are the absorbances of **RuRe**, of which the initial concentration was 50 μM in 50 mL of MeCN, in the filtrates before and after the adsorption procedure (the washing solvent was added into the filtrate, and the amount of the solution was adjusted to be the same, i.e., 50 mL) and X is the amount of Al_2O_3 particles added. Figure 1 shows the

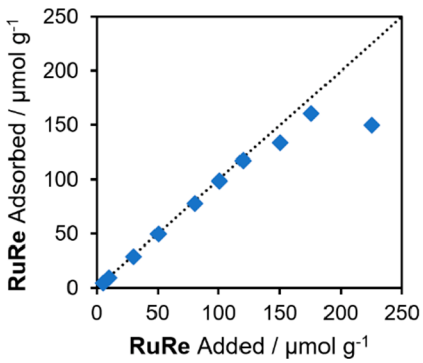

Figure 1. Adsorption amounts of **RuRe** on Al_2O_3.

adsorption curve for **RuRe** on Al_2O_3 surfaces. Almost all of the dissolved **RuRe** in the solution is adsorbed onto Al_2O_3 when AA is below 110 μmol g^{-1}, and the maximum is AA = 130 μmol g^{-1}.

Surface coverages of **RuRe** on Al_2O_3 (SC) were estimated using eq 4 where R is the short molecular radius of **RuRe** (R = 0.6 nm) calculated using the MM2 molecular mechanics program (Figure 2).

$$\mathrm{SC}\ (\%) = \frac{\mathrm{AA}\ (\mu\mathrm{mol\ g^{-1}}) \times R^2 \times 3.14 \times N_A}{\text{specific surface area}\ (\mathrm{m^2\ g^{-1}})} \times 100 \tag{4}$$

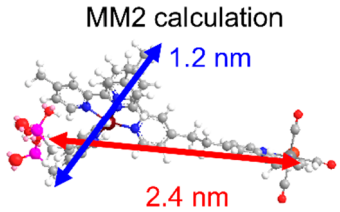

Figure 2. Molecular lengths of **RuRe** optimized by MM2 calculation.

The specific surface area was measured by nitrogen adsorption/desorption isotherm analysis and the Brunauer−Emmett−Teller equation (Figure S1). For example, the SC of the sample with AA = 130 μmol g^{-1} was calculated as 93 ± 9%. This suggests that the Al_2O_3 surface of this sample is very densely covered, even with a single layer of **RuRe**. The AA (SC) value was reproductively controlled between 5 μmol g^{-1} (5%) and 110 μmol g^{-1} (80%) by changing the amount of Al_2O_3 added into the **RuRe** solution.

Figure 3a shows the diffuse reflectance FT-IR spectrum of **RuRe**/Al_2O_3 (AA = 5 μmol g^{-1}). CO stretching bands of the Re unit are observed at ν(CO) = 2022, 1910, and 1900 cm^{-1}, which is in agreement with the FT-IR absorption spectrum of **RuRe** measured in MeCN solution. Figure 3b shows the diffuse reflectance UV−vis spectrum of **RuRe**/Al_2O_3 (AA = 5 μmol g^{-1}) and the UV−vis absorption spectrum of **RuRe** in MeCN. Absorption bands attributed to singlet metal-to-ligand charge transfer (^{1}MLCT) absorption were observed at around 460 nm in both spectra.

The coadsorption of both **Ru** and **Re** onto Al_2O_3 was performed according to the following stepwise procedure because of the low solubility of **Re** in MeCN: First, the Al_2O_3 particles were added to a MeOH solution containing **Re**, and the solution was stirred at room temperature for 7 days. The dispersion was filtered, and the obtained solid was washed using MeOH. The solid was added into an MeCN solution containing **Ru**, and the solution was stirred again for 7 days. The same subsequent filtration and washing procedures were used to obtain (**Ru** + **Re**)/Al_2O_3, and the desorption of the complexes was measured by the same procedure as that used for **RuRe**/Al_2O_3. The desorption was found to be very low (<4%).

Photocatalytic CO_2 reduction was carried out as follows: The **RuRe**/Al_2O_3 particles were dispersed in DMA−TEOA (4:1, v/v) containing 1-benzyl-1,4-dihydronicotinamide (BNAH) as a one-electron donor at a concentration of 0.1 M. These suspensions were saturated with CO_2 and irradiated at λ_{ex} > 480 nm using a high-pressure Hg lamp equipped with a K_2CrO_4 (30% w/w, d = 1 cm) aqueous solution filter. In each sample, the amount of the photosensitizer unit in the photocatalytic reaction was adjusted to 100 nmol. For example, the amounts of **RuRe**/Al_2O_3 particles added were 20 and 2 mg for AA = 5 and 50 μmol g^{-1}, respectively. To minimalize the differences between the dispersed reaction solutions due to the effect of light scattering, untreated Al_2O_3 particles were additionally introduced into the reaction solution to make the total amount of **RuRe**/Al_2O_3 and Al_2O_3 20 mg. During irradiation, the reaction solution was stirred using a magnetic stirrer.

https://dx.doi.org/10.1021/jacs.0c09170
J. Am. Chem. Soc. XXXX, XXX, XXX−XXX

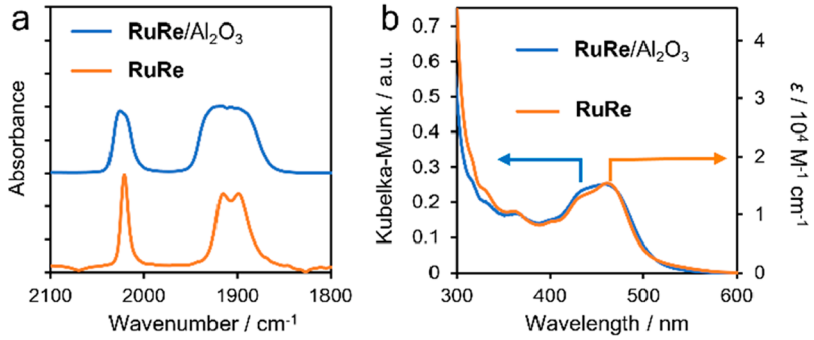

Figure 3. (a) FT-IR spectra of **RuRe** adsorbed on Al_2O_3 and **RuRe** dissolved in MeCN. (b) UV−vis diffuse reflectance and absorption spectra of **RuRe**/Al_2O_3 and **RuRe**.

Figure 4 shows the time profiles of product generation in photochemical CO_2 reduction using **RuRe**/Al_2O_3 (a and b) and (**Ru** + **Re**)/Al_2O_3 (c and d), for which AA is (5 and 5 μmol g^{-1}) and (50 and 50 μmol g^{-1}). In both cases using **RuRe**/Al_2O_3, CO was photocatalytically produced as a major product with high selectivity (Γ_{CO} = 80% and 92%) and relatively high turnover numbers (TON_{CO} = 60 and 86, respectively). It is important to note that the photocatalytic reduction of CO_2 proceeded even in the system using **RuRe**/Al_2O_3 with very low AA (Figure 4a), where the distance between the neighboring **RuRe** molecules on the Al_2O_3 is much larger than the molecular size of **RuRe**, as described later, and BNAH can provide only one electron upon excitation of the photosensitizer unit of **RuRe** because the one-electron oxidized and deprotonated compound, i.e., BNA$^{\bullet}$, quickly dimerizes to 4,4′-BNA_2 or 4,6′-BNA_2 (eq 5), neither of

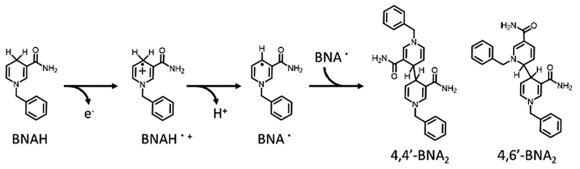

(5)

which can reduce **RuRe** in the ground state. Therefore, we can conclude that the photocatalytic CO formation proceeds via step-by-step double excitations of the photosensitizer unit of **RuRe** in the ground state, which are followed by reductive quenching processes of its excited state by BNAH each time, for an isolated **RuRe** molecule on Al_2O_3.

Although CO was also photocatalytically produced over (**Ru** + **Re**)/Al_2O_3 with both higher AAs (Figure 4d: AA = 50 μmol g^{-1} and 50 μmol g^{-1}), the TON_{CO} and Γ_{CO} values were much lower (TON_{CO} = 25, Γ_{CO} = 85%) than those for the supramolecular systems (TON_{CO} = 86, Γ_{CO} = 92%). For the lower-adsorption-density case (Figure 4c: AA = 5 μmol g^{-1}), the effectiveness of the supramolecular photocatalyst was more apparent: TON_{CO} = 60 and Γ_{CO} = 80% in the system using **RuRe**/Al_2O_3 while TON_{CO} = 5 and Γ_{CO} = 32% in the system using (**Ru** + **Re**)/Al_2O_3. These results clearly indicate that the covalent bonding between the Ru photosensitizer and Re catalyst units in the supramolecular photocatalysts plays a crucial role in the photocatalytic CO_2 reduction on the solid surface. It has been reported that rapid electron transfer proceeds from the one-electron-reduced Ru photosensitizer unit, which is produced by photochemical reductive quenching, to the Re catalyst unit in the supramolecular photocatalyst systems in solution, and this process is a through-bond electron transfer.[22,23]

In the cases of the mixed mononuclear system, i.e., (**Ru** + **Re**)/Al_2O_3, only intermolecular electron transfer from the reduced **Ru** to **Re** can trigger the photocatalytic reaction, which is therefore slower or not possible, especially in the low-AA case. Photocatalytic CO formation did not proceed in the cases using only **Ru** or **Re** adsorbed on Al_2O_3 (**Ru**/Al_2O_3, **Re**/Al_2O_3, Figure S2).

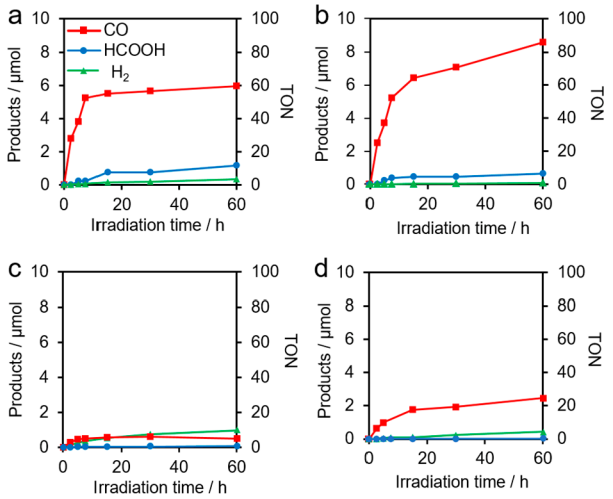

Figure 4. Time profiles of CO (red), HCOOH (blue), and H_2 (green) production during photocatalytic reactions over (a) **RuRe**/Al_2O_3 (AA = 5 μmol g^{-1}), (b) **RuRe**/Al_2O_3 (AA = 50 μmol g^{-1}), (c) (**Ru** + **Re**)/Al_2O_3 (AA = 5 + 5 μmol g^{-1}), and (d) (**Ru** + **Re**)/Al_2O_3 (AA = 50 + 50 μmol g^{-1}).

Figure 5 shows the time profile for the TON values of CO formation in the photocatalytic reaction using **RuRe**/Al_2O_3 with various AAvalues (5−110 μmol g^{-1}). In all cases, CO was produced with high selectively (Γ_{CO} > 80%) with 60 h of light irradiation, and small amounts of HCOOH and H_2 were detected as minor products. Both the turnover number and frequency of CO formation (TON_{CO} and TOF_{CO}) showed different trends depending on the AA. We can assess the durabilities of the **RuRe**/Al_2O_3 systems using the TON_{CO} values obtained after 120 h irradiation. Conversely, the TOF_{CO} value in the initial stage of the reaction can be used as an indicator of the rate of CO formation, which here is defined as the value of the TON_{CO} value at 1 h of irradiation. The data are summarized in Table 1. The TOF_{CO} was lower in the case

https://dx.doi.org/10.1021/jacs.0c09170
J. Am. Chem. Soc. XXXX, XXX, XXX−XXX

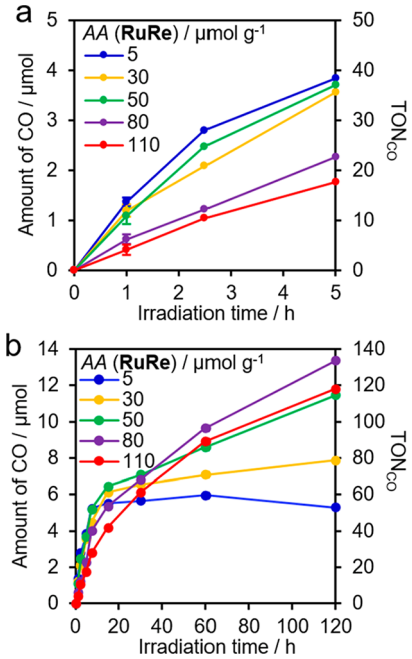

Figure 5. Time courses of CO formation during the photocatalytic reactions using **RuRe**/Al_2O_3 with different AA values during irradiation at λ_{ex} > 480 nm in DMA/TEOA (4:1, v/v) containing BNAH (0.1 M) under CO_2 atmosphere (a) up to 5 h irradiation and (b) up to 120 h irradiation.

with the higher AA (for example, 14 h^{-1} at 5 μmol g^{-1} and 4 h^{-1} at 110 μmol g^{-1}). Interestingly, TON_{CO} was higher for higher AA up to AA = 80 μmol g^{-1} (56 at 5 μmol g^{-1} and 134 at 80 μmol g^{-1}). Although in the case for AA = 110 μmol g^{-1}, TON_{CO} was slightly lower than that for AA = 80 μmol g^{-1}, and it was still higher than that for the other cases (TON_{CO} = 118).

Data for emission from the Ru(II) photosensitizer unit on the Al_2O_3 and its quenching by BNAH are summarized in Table 1. The quenching fraction (η_q) indicates how much the photosensitizer excited state was reductively quenched by BNAH (0.1 M) and is calculated using eq 6 with the Stern−Volmer constant (K_{SV}).

$$\eta_q = \frac{0.1 \times K_{SV}}{1 + 0.1 \times K_{SV}} \tag{6}$$

Although all emission decays from the excited **RuRe**/Al_2O_3 in suspended solutions could be reasonably fitted by using a single exponential function (Figure S3), the obtained emission lifetime (τ_{em}) was dependent on AA; i.e., a higher AA led to a shorter τ_{em}. For example, τ = 762 ns at AA = 5 μmol g^{-1} and τ = 685 ns at AA = 110 μmol g^{-1}. However, the emission lifetime did not change upon decreasing the intensity of the excitation light using a 10% neutral density filter. Therefore, triplet−triplet annihilation should not proceed. The rate constants of nonradiative and radiative deactivation (k_r and k_{nr}) were calculated using the values of the emission quantum yield and the emission lifetime: k_{nr} increased with increasing adsorption density while k_r did not change. These results strongly suggest that self-quenching occurred on the Al_2O_3 surface. This is likely to be one of the reasons for the lower η_q value in the cases with higher AA.

Figure 6 shows the Stern−Volmer plots for the quenching of emissions from **RuRe**/Al_2O_3 by BNAH, all of which exhibited

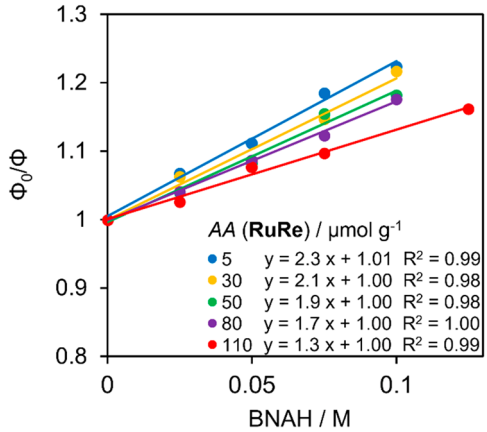

Figure 6. Stern−Volmer plots of the quenching of emission from **RuRe** on Al_2O_3 surfaces at different adsorption densities. Excitation wavelength = 510 nm. The solvent was DMA/TEOA (4:1, v/v).

good linearity, thus giving the reductive quenching rate constant of the excited Ru(II) photosensitizer unit on the Al_2O_3 (k_q in Table 1). The k_q value also decreased when the AA increased. This suggests that a higher adsorption density of **RuRe** on Al_2O_3 caused a higher steric interaction among the neighboring **RuRe** molecules on Al_2O_3, hindering the approach of BNAH to the excited Ru photosensitizer unit owing to the bulkiness of the Re unit. The slower reductive quenching should also lower the TOF_{CO} value. It is noteworthy that BNAH acts as a one-electron donor with the one-photon

Table 1. Photophysical, Quenching, and Photocatalytic Behaviors of RuRe/Al_2O_3[a]

AA, μmol g^{-1}	τ, ns[b]	Φ_{em}	k_r, 10^5 s^{-1}[c]	k_{nr}, 10^5 s^{-1}[d]	K_{SV}, M^{-1}	η_q[e]	k_q, 10^6 M^{-1} s^{-1}	TOF_{CO}, h^{-1}[f]	TON_{CO}	Γ_{CO}, %[g]	r, nm[h]
5	762	0.12	1.5	11.6	2.3	0.19	3.0	14	56	68	6.3
30	711	0.11	1.5	12.6	2.1	0.17	2.9	12	78	85	2.6
50	695	0.10	1.5	12.9	1.9	0.16	2.8	11	115	93	2.0
80	687	0.10	1.5	13.0	1.7	0.15	2.5	6	134	98	1.6
110	685	0.10	1.5	13.1	1.3	0.12	1.9	4	118	98	1.3
5 and 95[i]	550	0.08	1.5	16.7	2.0	0.17	3.6	48	707[j]	91	1.4

[a]A DMA/TEOA mixed solution (4:1, v/v) under CO_2. [b]λ_{ex} = 510 nm. [c]Rate constants for radiative deactivation calculated as $k_r = \Phi_{em}/\tau_{em}$. [d]Rate constants for nonradiative deactivation calculated as $k_{nr} = k_r/\Phi_{em} - k_r$. [e]Quenching fraction in the presence of BNAH (0.1 M). [f]TOF_{CO} calculated as [produced CO during initial 1 h (mol)]/[used **RuRe** (mol) × irradiation time (h)]. [g]Selectivity of CO formation calculated as (produced CO)/(total of CO, HCOOH, and H_2) at 120 h. [h]Average distance between metal complexes calculated as [(specific surface area (m^2 g^{-1}))/(adsorption density (mol g^{-1}) × N_A × 3.14)]1/2 × 2. [i](**RuRe** + **Ru**)/Al_2O_3. [j]Based on **RuRe** used. The data after irradiation for 60 h.

https://dx.doi.org/10.1021/jacs.0c09170
J. Am. Chem. Soc. XXXX, XXX, XXX−XXX

excitation of the Ru photosensitizer unit because of the rapid dimerization of BNA• (eq 5). However, since CO formation from CO_2 requires two-electron reduction, the reductive quenching of the excited Ru photosensitizer unit by BNAH should proceed twice. Therefore, these higher AA values may have multiple effects on lowering TOF_{CO}.

For long irradiation times, the durability of **RuRe**/Al_2O_3 increases upon increasing AA (Figure 5). For example, at AA = 5 μmol g^{-1}, photocatalytic CO formation was terminated after 15 h irradiation with $TON_{CO} \sim 60$. Conversely, the sample with AA = 110 μmol g^{-1} continuously produced CO for over 120 h, and TON_{CO} was 118 after 120 h irradiation. It is noteworthy that the initial speed of the CO formation over **RuRe**/Al_2O_3 with AA = 110 μmol g^{-1} was much slower than that with AA = 5 μmol g^{-1}. Therefore, the formation amounts were reversed after ~30 h irradiation. The rapid termination of the photocatalytic CO formation was observed when AA $\leq$ 30 μmol g^{-1}, while the photocatalysis continued for longer when AA $\geq$ 50 μmol g^{-1}, especially at 80−110 μmol g^{-1}. Table 1 summarizes TON_{CO} after 120 h irradiation using **RuRe**/Al_2O_3 with various AA values.

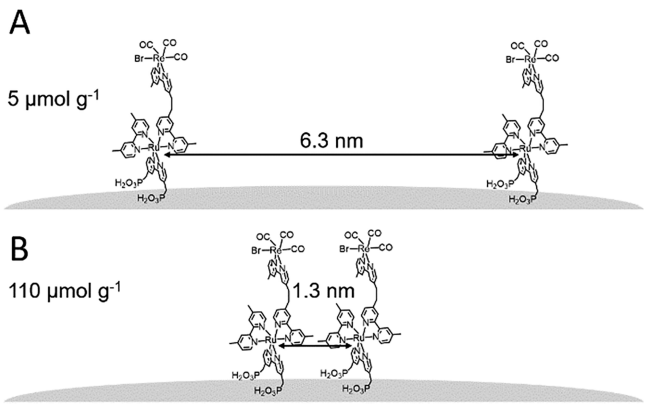

Figure 7. Average metal-to-metal distances for **RuRe**. (A) Average distance between **RuRe** at 5 μmol g^{-1}. (B) Average distance between **RuRe** at 110 μmol g^{-1}.

The average distance between the centers of neighboring **RuRe** molecules on Al_2O_3 (r) is calculated using eq 7 (Table 1).

$$r = \sqrt{\frac{\text{specific surface area } (m^2 g^{-1})}{\text{AA } (\text{mol } g^{-1}) \times N_A \times 3.14}} \times 2 \quad (7)$$

For example, r is 1.3 and 6.3 nm when AA is 110 and 5 μmol g^{-1}, respectively (Figure 7). Thus, rapid termination of photocatalytic CO formation was observed when $r \geq 2.6$ nm, while the photocatalysis continued for an extended duration when $r \leq 2.0$ nm, especially 1.3−1.6 nm. The molecular dimensions of **RuRe** (Figure 2) are 1.2 nm (diameter of the Ru photosensitizer unit) and 2.4 nm (length along the bond between the Ru and Re units). These results indicate that the durability of the photocatalyst decreased when the average distance between the **RuRe** molecules on Al_2O_3 was longer than the length of **RuRe** (Figure 7).

The dispersion after the photocatalytic reaction for 30 h was filtered, and the obtained solid was dispersed again into a DMA/TEOA (4:1, v/v) solution in the absence of BNAH in order to measure the emission quantum yields from the Ru photosensitizer unit (Φ_{em}). Figure 8 shows Φ_{em} for the **RuRe**/

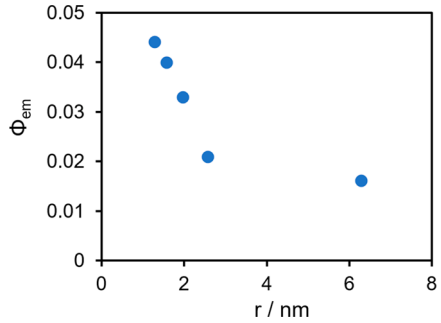

Figure 8. Relationship between Φ_{em} and the average inter-**RuRe** distance for **RuRe**/Al_2O_3 after 30 h of photocatalytic reaction in DMA/TEOA (4:1, v/v) at 480 nm excitation under a CO_2 atmosphere.

Al_2O_3 samples with various r values. Φ_{em} drastically decreased with the r value when $r < 2.6$ nm, and the Φ_{em} values for r = 2.6 and 6.3 nm were similar and lower than the others. It is noteworthy that the emission efficiencies of the sample with the larger r value before the photocatalysis tended to be higher, and all of the values were higher than those after the photocatalytic reaction (Table 1). It has been reported that photochemical ligand substitution of the Ru photosensitizer unit occurs when one-electron-reduced species (OERS) of the Ru photosensitizer are excited in solution.[46] The products were $[Ru(diimine)_2(solvent)_2]^{2+}$-type complexes, which do not emit at room temperature in solution.

The suspensions after photocatalytic reactions for 0, 30, and 60 h were filtered, and the diffuse reflectance UV−vis spectra of the obtained solid samples were measured (Figure 9). In the case of AA = 5 μmol g^{-1}, the broad absorption at the 460 nm, which is attributed to the ^{1}MLCT band of the Ru photosensitizer unit, decreases, and a new absorption at longer wavelength appears. This also strongly indicates that ligand substitution of the Ru photosensitizer unit occurs during the photocatalytic reaction, giving the $[Ru(diimine)_2(solvent)_2]^{2+}$-type complex(es). In the case of AA = 110 μmol g^{-1}, such spectral changes were slower, as shown in Figure 9b.

The results presented above and those in previous reports dealing with homogeneous systems[18,46] strongly suggest that the decomposition, i.e., the ligand-substitution reaction of the Ru photosensitizer unit of **RuRe**, occurred during the photocatalytic reaction, especially for the **RuRe**/Al_2O_3 samples with $r \geq 2.6$ nm. This reaction induced loss of the photocatalytic activity of **RuRe**/Al_2O_3. In other words, higher r values led to more rapid decomposition of the Ru photosensitizer unit of **RuRe** on Al_2O_3, and this is most likely one of the main reasons that the durability of the photocatalyst is lower for **RuRe**/Al_2O_3 samples with higher r values, especially those with $r \geq 2.6$ nm. Therefore, the durability and photocatalytic activity of **RuRe** (except for the initial reductive quenching process of the excited **RuRe** by BNAH) could be increased by closely arranging the **RuRe** molecules on the Al_2O_3 surface. Since **RuRe** cannot move on the Al_2O_3 surface, it does not readily contact with other neighboring **RuRe** moieties at low adsorption density with $r > 2.6$ nm, which is similar to the molecule length along the bond between the Ru and Re units of **RuRe** (Figure 2). One possible mechanism for the increase in the photocatalyst durability upon introducing shorter distances between the **RuRe** molecules on Al_2O_3 is the donation of one electron from an OERS of **RuRe** to another OERS (disproportionation) and/or

https://dx.doi.org/10.1021/jacs.0c09170
J. Am. Chem. Soc. XXXX, XXX, XXX−XXX

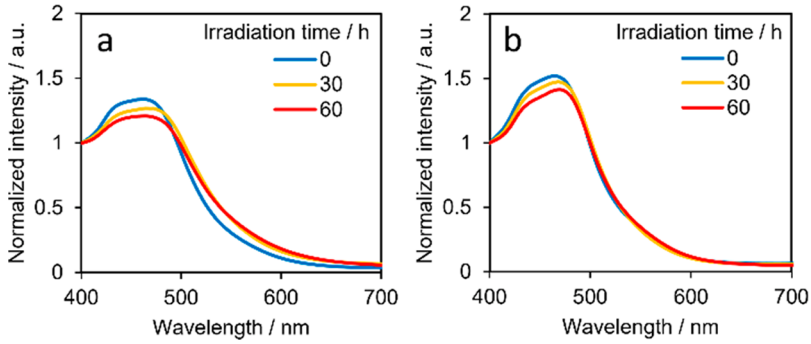

Figure 9. Diffuse reflectance UV−vis spectra of **RuRe**/Al_2O_3 after photocatalytic reaction: (a) 5 μmol g^{-1}; (b) 110 μmol g^{-1}. The spectra are normalized at 400 nm.

the intermediate derived from the OERS of **RuRe**, since CO formation from CO_2 requires two-electron reduction. To obtain two electrons via photochemical reduction of the complex(es) by BNAH, **RuRe** needs to be excited twice and quenched by BNAH each time. However, the side reaction and/or decomposition of the one-electron-reduced complexes may proceed before the second photon absorption during the photocatalytic reactions, even when using a high-power light source such as the 500 W high-pressure mercury lamp employed in the present study. If the neighboring OERS of **RuRe** can donate an electron to another OERS (or the intermediate), their reaction speed should increase in order to decrease the residence time of the OERS species in the reaction solution.

In order to clarify whether a second electron reduction donation process from an adjacent OERS species of **RuRe** accelerates the photocatalytic CO_2 reduction, a model mononuclear analogue of the Ru photosensitizer unit (**Ru**) was coadsorbed on **RuRe**/Al_2O_3. **RuRe**/Al_2O_3 (AA = 5 μmol g^{-1}) synthesized as described above was dispersed into MeCN solutions containing various concentrations of **Ru**, and the suspensions were stirred for 2 days. The codoped samples, labeled (**RuRe** + **Ru**)/Al_2O_3, were collected by filtration and washed in MeCN several times. The photocatalytic abilities of the dispersions of (**RuRe** + **Ru**)/Al_2O_3 (2 mg which contains 10 nmol of **RuRe**) in DMA/TEOA (4:1, v/v, 4 mL) solutions containing BNAH (0.1 M) were investigated (λ_{ex} > 480 nm under a CO_2 atmosphere), and Figure 10 shows the results. The photophysical and quenching behaviors of (**RuRe** + **Ru**)/Al_2O_3 (AA = 5 μmol g^{-1} and 95 μmol g^{-1}, respectively) are also summarized in Table 1. Since the formation amounts of CO in the initial stage of the photocatalytic reaction using 2 mg of **RuRe**/Al_2O_3, which contained 10 mg of **RuRe** in the absence of **Ru**, were lower than the detection limit, in Figure 10, the data in the case using 100 nmol of **RuRe**, of which the solution contained 10 times more **RuRe**/Al_2O_3 (5 μmol g^{-1}) particles (Figure 4a), were divided by 10 and are shown as 0 μmol g^{-1} (blue plots) in Figure 10. The coadsorption of **Ru** clearly induced higher photocatalytic activity compared to that using **RuRe**/Al_2O_3 without **Ru** (CO formation: 0.60 μmol for 60 h irradiation). Upon increasing the amount of **Ru** on **RuRe**/Al_2O_3 from AA = 20 to 95 μmol g^{-1}, an increase in CO formation from 1.7 to 7.1 μmol at 60 h of light irradiation was observed. It should be noted that the system using **Ru**/Al_2O_3 (AA = 100 μmol g^{-1}) in the absence of **RuRe** produced only a small amount of CO (0.13 μmol, Figure S2), and the durability drastically increased when the total adsorption amounts of **RuRe** and **Ru** were AA ≥ 55 μmol g^{-1}, where the average

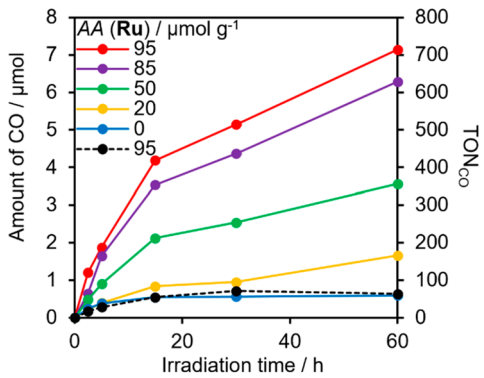

Figure 10. Time profile of TON_{CO} during photocatalytic reaction over (**RuRe** + **Ru**)/Al_2O_3 in DMA/TEOA (4:1, v/v) containing 0.1 M BNAH under a CO_2 atmosphere. Irradiation at λ_{ex} > 480 nm using a Hg lamp. In each sample, the adsorption density of **RuRe** was adjusted to AA = 5 μmol g^{-1}. The adsorption density of **Ru** was maintained at AA = 95 μmol g^{-1} (red), 85 μmol g^{-1} (purple), 50 μmol g^{-1} (green), 20 μmol g^{-1} (yellow), and 0 μmol g^{-1} (blue). The amount of **RuRe** was fixed at 10 nmol, which is much smaller compared to the case shown in Figure 4a (100 nmol). The black plots with dotted line show CO formation using (**Ru**+**Re**)/Al_2O_3 (AA = 95 and 5 μmol g^{-1}). The amounts of **Re** in all the samples were 10 nmol.

distance between the complexes is $r \leq 2$ nm. These results clearly indicate that the OERS species of **Ru**, which are produced upon photochemical reduction by BNAH, can donate one electron not only to **RuRe** but also to the OERS of **RuRe** and/or the intermediate derived from the OERS of **RuRe**. Consequently, consumption of the OERS of **RuRe** should be accelerated, and the durability of **RuRe** should be increased. Therefore, a similar process should also work in the case of photocatalytic reactions using **RuRe**/Al_2O_3; i.e., the OERS of **RuRe** donates one electron to another OERS (disproportionation) and/or the intermediate derived from the OERS of **RuRe** to allow two-electron reduction of CO_2 to CO. Interestingly, the photocatalytic ability of the sample with both the model mononuclear **Ru** and **Re** complexes with high adsorption density, i.e., (**Ru** + **Re**)/Al_2O_3 (both AAs = 50 μmol g^{-1}), was much lower than that of **RuRe** /Al_2O_3 (AA = 50 μmol g^{-1}) (Figures 4b and 4d), and, even at a low adsorption density such as AA = 5 μmol g^{-1} (r = 6.3 nm), **RuRe** works as a photocatalyst for CO_2 reduction. These results strongly suggest that CO formation via double excitation of the same Ru photosensitizer unit in one molecule of **RuRe** also proceeds as described previously. The bimolecular mechanism described in this section can accelerate

https://dx.doi.org/10.1021/jacs.0c09170
J. Am. Chem. Soc. XXXX, XXX, XXX−XXX

photocatalytic CO_2 reduction using **RuRe**. The black plots with a dotted line in Figure 10 show CO formation in the system using (**Ru** + **Re**)/Al_2O_3 (AA = 95 and 5 μmol g^{-1}) (TON_{CO} was 64 after irradiation for 60 h), which was much lower compared to that in the case using (**RuRe** + **Ru**)/Al_2O_3 with the same amount of **Ru** adsorbed sample (red plots in Figure 10, Table 1). This result clearly indicates that connection between the photosensitizer and the catalyst using the bridging ligand is important for improving photocatalysis even on the solid surface probably due to the rapid electron transfer from the OERS of the photosensitizer unit to the catalyst unit via though-bond electron transfer (within several nanoseconds).[22]

It is noteworthy that the amount of CO formation in the case using (**RuRe** + **Ru**)/Al_2O_3, which contained only 10 nmol of **RuRe**, could produce over 7 μmol of CO for 60 h irradiation with the assistance of the coadsorbed **Ru** (190 nmol). It is a larger amount than that produced by using a 10 times higher amount of **RuRe** in the case of **RuRe**/Al_2O_3 with AA = 5 μmol g^{-1} (5.6 μmol of CO formation). It should be also noted that the TOF_{CO} of (**RuRe** + **Ru**)/Al_2O_3 (AA = 5 and 95 μmol g^{-1}) (TOF_{CO} = 48) was much higher than those in the cases using **RuRe**/Al_2O_3 (Table 1). It is also noteworthy that the k_q value of (**RuRe** + **Ru**)/Al_2O_3 (AA = 5 and 95 μmol g^{-1}) was larger even compared to that of **RuRe**/Al_2O_3 (AA = 5 μmol g^{-1}) even though the redox potential of the excited **Ru** should be very similar to that of the excited Ru unit of **RuRe** (Table 1). This clearly indicates that the steric hindrance made by the Re unit on the surface of Al_2O_3 makes reductive quenching of the excited Ru unit less efficient in **RuRe**; in other words, the coadsorption of **Ru** can make both durability and efficiency of **RuRe** as the photocatalyst much better. Coadsorption of redox photosensitizers can reinforce the photocatalysis of the supramolecular photocatalyst.

■ CONCLUSIONS

A dinuclear complex consisting of Ru(II) photosensitizer and Re(I) catalyst units, **RuRe**, fixed on an Al_2O_3 surface can photocatalyze CO_2 reduction with high selectivity for CO formation. The photocatalytic ability of this system is much higher than that using a mixture of the corresponding mononuclear complexes fixed on the same Al_2O_3 surface, i.e., (**Re** + **Ru**)/Al_2O_3. This clearly demonstrates the superiority of the supramolecular photocatalyst, in which the photosensitizer and catalyst complexes are connected with an ethylene chain, compared to the corresponding mixed system consisting of mononuclear photosensitizer and catalyst complexes fixed on a solid surface. The rapid intramolecular electron transfer from the photochemically reduced photosensitizer unit to the catalyst unit plays an important role in the superiority of the supramolecular photocatalyst, especially on the surface of the solid material. The photocatalytic CO formation proceeds via step-by-step double excitations of the same Ru photosensitizer unit in one molecule of **RuRe** followed by the reductive quenching of the excited state by BNAH each time, at least in the case of a **RuRe** molecule isolated on Al_2O_3.

The speed and durability of the photocatalysis were strongly and oppositely dependent on the distance (r) between the neighboring **RuRe** molecules; i.e., shorter r induced slower CO formation in the initial stage of the photocatalytic reaction but higher durability at longer irradiation time. Steric hindrance between neighboring **RuRe** molecules owing to the short r suppresses the access of the reductant (BNAH) to the excited photosensitizer unit, lowering the quenching fraction (η_q) and suppressing the production yield of the OERS of **RuRe**. However, when r is equal to or shorter than the distance over which neighboring **RuRe** molecules can contact with each other, another mechanism of the photocatalytic reduction of CO_2 comes into play. This mechanism proceeds via the disproportionation of two OERSs of **RuRe** and/or electron donation from the OERS of **RuRe** to the intermediate.

Based on these investigations, we could successfully construct an efficient and durable photocatalytic system for CO_2 reduction using a minimal amount of Re metal, i.e., coadsorption of a small amount of **RuRe** with an excess amount of the photosensitizer mononuclear complex (**Ru**) on Al_2O_3.

These investigations provide new architectures for the construction of efficient and durable hybrid photocatalytic systems composed of metal-complex photocatalysts and solid materials for CO_2 reduction; e.g., the chemical bonding between a redox photosensitizer and a catalyst, i.e., the supramolecular photocatalyst structure, has big advantages compared to the mixed system of the corresponding mononuclear complexes on a solid surface, and second electron donation to the reduced catalyst unit from outside can drastically increase the durability of the supramolecular photocatalyst.

■ EXPERIMENTAL SECTION

General Procedures. ^{1}H NMR spectra were measured using a JEOL ECA-400II. For the measurement of ^{31}P NMR, a JEOL LA400 was used. A Shimadzu LCMS-2010A was used for electrospray ionization mass spectrometry (ESI-MS). A JASCO V-670 was used for UV−vis absorption spectra and diffuse reflection UV−vis spectra. A quartz cell (optical path length of 1 cm) and a reflection measurement unit (JASCO, sample part Φ = 5 mm) equipped with an integrating sphere were used, respectively. Emission quantum yields were determined using a Hamamatsu Photonics absolute PL quantum yield measurement system C9920-01 (excitation light source: 150 W Xe lamp; detector: PMA-12 multichannel CCD). Emission lifetimes were obtained using a Horiba FluoroHub time-correlated singl-photon-counting system. The excitation light source was an LED pulse lamp (NanoLED, 510 nm), and a TBX-04. BELLSORP-miniII was used for nitrogen adsorption/desorption measurement (measurement temperature: 77 K). Brunauer−Emmett−Teller (BET) specific surface areas were calculated from values in the region where the relative pressure was 0.08−0.2 in the adsorption isotherm after heating at 333 K for 2 h.

All chemicals and solvents were commercial reagent quality and used without purification unless otherwise stated. DMA was dried over 4 Å molecular sieves and distilled under reduced pressure. TEOA was distilled under reduced pressure. BNAH was synthesized according to the literature procedure.[47]

Synthesis of RuRe, Ru, and Re Adsorbed on Al_2O_3. The **RuRe**, **Ru**, and **Re** were synthesized according to the previously reported method.[41,44,45] The desired amount of Al_2O_3 was dispersed in acetonitrile (20 mL), and another acetonitrile solution containing the metal complex (50 μM) was added into it. This suspension was stirred for 1 week under an Ar atmosphere. The suspension was filtered, and the obtained solid was washed with acetonitrile several times.

Photocatalytic Reactions. Photocatalytic reactions were performed using 11 mL test tubes. DMA/TEOA (4:1, v/v) solutions (4 mL) containing BNAH (0.1 M) were bubbled with CO_2 for 20−30 min in a test tube and then dispersed using a magnetic stirrer. A high-pressure Hg lamp (300 W, Eikosya Co.) equipped with a uranyl glass and a K_2CrO_4 solution filter (λ < 480 nm) were used as a light source. During irradiation, the reaction solution was stirred and kept at approximately 25 °C using a constant-temperature water tank. The

https://dx.doi.org/10.1021/jacs.0c09170
J. Am. Chem. Soc. XXXX, XXX, XXX−XXX

produced CO and H_2 were analyzed by a GC-TCD (GL science GC323). Formic acid was analyzed using a capillary electrophoresis system (Agilent 7100) with a buffer solution (pH = 6.0) consisting of quinolinic acid, hexadecyltrimethylammonium hydroxide, and 2-amino-2-hydroxymethyl-1,3-propanediol as the electrolyte.

■ ASSOCIATED CONTENT

Supporting Information

The Supporting Information is available free of charge at https://pubs.acs.org/doi/10.1021/jacs.0c09170.

Adsorption/desorption isotherm for Al_2O_3; time courses of CO, HCOOH, and H_2 using **Re**/Al_2O_3 and **Ru**/Al_2O_3; emission decay curves for **RuRe**/Al_2O_3 (PDF)

■ AUTHOR INFORMATION

Corresponding Author

Osamu Ishitani − *Department of Chemistry, Tokyo Institute of Technology, Meguro-ku, Tokyo 152-8550, Japan;* orcid.org/0000-0001-9557-7854; Email: ishitani@chem.titech.ac.jp

Authors

Daiki Saito − *Department of Chemistry, Tokyo Institute of Technology, Meguro-ku, Tokyo 152-8550, Japan*

Yasuomi Yamazaki − *Department of Chemistry, Tokyo Institute of Technology, Meguro-ku, Tokyo 152-8550, Japan;* orcid.org/0000-0002-8640-7367

Yusuke Tamaki − *Department of Chemistry, Tokyo Institute of Technology, Meguro-ku, Tokyo 152-8550, Japan*

Complete contact information is available at: https://pubs.acs.org/10.1021/jacs.0c09170

Notes

The authors declare no competing financial interest.

■ ACKNOWLEDGMENTS

This work was supported by JSPS KAKENHI Grant Number JP20H00396 and JP17H06440 in Scientific Research on Innovative Areas "Innovations for Light-Energy Conversion (I4LEC)".

■ REFERENCES

(1) Schwarz, H. A.; Dodson, R. W. Reduction potentials of CO_2^- and the alcohol radicals. *J. Phys. Chem.* **1989**, *93*, 409−414.

(2) Koppenol, W. H.; Rush, J. D. Reduction potential of the carbon dioxide/carbon dioxide radical anion: a comparison with other C1 radicals. *J. Phys. Chem.* **1987**, *91*, 4429−4430.

(3) Lehn, J.-M.; Ziessel, R. Photochemical generation of carbon monoxide and hydrogen by reduction of carbon dioxide and water under visible light irradiation. *Proc. Natl. Acad. Sci. U. S. A.* **1982**, *79*, 701−704.

(4) Hawecker, J.; Lehn, J.-M.; Ziessel, R. Electrocatalytic reduction of carbon dioxide mediated by Re(bipy)$(CO)_3$Cl (bipy = 2,2′-bipyridine). *J. Chem. Soc., Chem. Commun.* **1984**, 328−330.

(5) Hawecker, J.; Lehn, J.-M.; Ziessel, R. Efficient photochemical reduction of CO_2 to CO by visible light irradiation of systems containing Re(bipy)$(CO)_3$X or Ru$(bipy)_3^{2+}$-Co^{2+} combinations as homogeneous catalysts. *J. Chem. Soc., Chem. Commun.* **1983**, 536−538.

(6) Ishida, H.; Tanaka, K.; Tanaka, T. The Electrochemical Reduction of CO_2 Catalyzed By Ruthenium Carbonyl Complexes. *Chem. Lett.* **1985**, *14*, 405−406.

(7) Lehn, J. M.; Ziessel, R. Photochemical reduction of carbon dioxide to formate catalyzed by 2,2t′-bipyridine- or 1,10-phenanthroline-ruthenium(II) complexes. *J. Organomet. Chem.* **1990**, *382*, 157−173.

(8) Bourrez, M.; Molton, F.; Chardon-Noblat, S.; Deronzier, A. [Mn(bipyridyl)$(CO)_3$Br]: An Abundant Metal Carbonyl Complex as Efficient Electrocatalyst for CO_2 Reduction. *Angew. Chem., Int. Ed.* **2011**, *50*, 9903−9906.

(9) Sullivan, B. P.; Bolinger, C. M.; Conrad, D.; Vining, W. J.; Meyer, T. J. One- and two-electron pathways in the electrocatalytic reduction of CO_2 by fac-Re(bpy)$(CO)_3$Cl (bpy = 2,2′-bipyridine). *J. Chem. Soc., Chem. Commun.* **1985**, 1414−1416.

(10) Fujita, E. Photochemical carbon dioxide reduction with metal complexes. *Coord. Chem. Rev.* **1999**, *185*−*186*, 373−384.

(11) Kuramochi, Y.; Ishitani, O.; Ishida, H. Reaction mechanisms of catalytic photochemical CO_2 reduction using Re(I) and Ru(II) complexes. *Coord. Chem. Rev.* **2018**, *373*, 333−356.

(12) Yamazaki, Y.; Takeda, H.; Ishitani, O. Photocatalytic reduction of CO_2 using metal complexes. *J. Photochem. Photobiol., C* **2015**, *25*, 106−137.

(13) Takeda, H.; Cometto, C.; Ishitani, O.; Robert, M. Electrons, Photons, Protons and Earth-Abundant Metal Complexes for Molecular Catalysis of CO_2 Reduction. *ACS Catal.* **2017**, *7*, 70−88.

(14) Bonin, J.; Maurin, A.; Robert, M. Molecular catalysis of the electrochemical and photochemical reduction of CO_2 with Fe and Co metal based complexes. Recent advances. *Coord. Chem. Rev.* **2017**, *334*, 184−198.

(15) Ghosh, D.; Takeda, H.; Fabry, D. C.; Tamaki, Y.; Ishitani, O. Supramolecular Photocatalyst with a Rh(III)-Complex Catalyst Unit for CO_2 Reduction. *ACS Sustainable Chem. Eng.* **2019**, *7*, 2648−2657.

(16) Kuramochi, Y.; Fujisawa, Y.; Satake, A. Photocatalytic CO_2 Reduction Mediated by Electron Transfer via the Excited Triplet State of Zn(II) Porphyrin. *J. Am. Chem. Soc.* **2020**, *142*, 705−709.

(17) Fabry, D. C.; Koizumi, H.; Ghosh, D.; Yamazaki, Y.; Takeda, H.; Tamaki, Y.; Ishitani, O. A Ru(II)-Mn(I) Supramolecular Photocatalyst for CO_2 Reduction. *Organometallics* **2020**, *39*, 1511−1518.

(18) Umemoto, A.; Yamazaki, Y.; Saito, D.; Tamaki, Y.; Ishitani, O. Synthesis of a Novel Re(I)-Ru(II)-Re(I) Trinuclear Complex as an Effective Photocatalyst for CO_2 Reduction. *Bull. Chem. Soc. Jpn.* **2020**, *93*, 127−137.

(19) Cheung, P. L.; Kapper, S. C.; Zeng, T.; Thompson, M. E.; Kubiak, C. P. Improving Photocatalysis for the Reduction of CO_2 through Non-covalent Supramolecular Assembly. *J. Am. Chem. Soc.* **2019**, *141*, 14961−14965.

(20) Tamaki, Y.; Ishitani, O. Supramolecular Photocatalysts for the Reduction of CO_2. *ACS Catal.* **2017**, *7*, 3394−3409.

(21) Cancelliere, A. M.; Puntoriero, F.; Serroni, S.; Campagna, S.; Tamaki, Y.; Saito, D.; Ishitani, O. Efficient trinuclear Ru(ii)-Re(i) supramolecular photocatalysts for CO_2 reduction based on a new tris-chelating bridging ligand built around a central aromatic ring. *Chem. Sci.* **2020**, *11*, 1556−1563.

(22) Yamazaki, Y.; Ohkubo, K.; Saito, D.; Yatsu, T.; Tamaki, Y.; Tanaka, S.; Koike, K.; Onda, K.; Ishitani, O. Kinetics and Mechanism of Intramolecular Electron Transfer in Ru(II)-Re(I) Supramolecular CO_2-Reduction Photocatalysts: Effects of Bridging Ligands. *Inorg. Chem.* **2019**, *58*, 11480−11492.

(23) Koike, K.; Grills, D. C.; Tamaki, Y.; Fujita, E.; Okubo, K.; Yamazaki, Y.; Saigo, M.; Mukuta, T.; Onda, K.; Ishitani, O. Investigation of excited state, reductive quenching, and intramolecular electron transfer of Ru(II)-Re(I) supramolecular photocatalysts for CO_2 reduction using time-resolved IR measurements. *Chem. Sci.* **2018**, *9*, 2961−2974.

(24) Sato, S.; Morikawa, T.; Saeki, S.; Kajino, T.; Motohiro, T. Visible-Light-Induced Selective CO_2 Reduction Utilizing a Ruthenium Complex Electrocatalyst Linked to a p-Type Nitrogen-Doped Ta_2O_5 Semiconductor. *Angew. Chem., Int. Ed.* **2010**, *49*, 5101−5105.

(25) Suzuki, T. M.; Yoshino, S.; Takayama, T.; Iwase, A.; Kudo, A.; Morikawa, T. Z-Schematic and visible-light-driven CO_2 reduction using H_2O as an electron donor by a particulate mixture of a Ru-complex/$(CuGa)_{1-x}Zn_{2x}S_2$ hybrid catalyst, $BiVO_4$ and an electron mediator. *Chem. Commun.* **2018**, *54*, 10199−10202.

(26) Kuehnel, M. F.; Orchard, K. L.; Dalle, K. E.; Reisner, E. Selective Photocatalytic CO_2 Reduction in Water through Anchoring of a Molecular Ni Catalyst on CdS Nanocrystals. *J. Am. Chem. Soc.* **2017**, *139*, 7217−7223.
(27) Schreier, M.; Luo, J.; Gao, P.; Moehl, T.; Mayer, M. T.; Grätzel, M. Covalent Immobilization of a Molecular Catalyst on Cu_2O Photocathodes for CO_2 Reduction. *J. Am. Chem. Soc.* **2016**, *138*, 1938−1946.
(28) Ma, B.; Chen, G.; Fave, C.; Chen, L.; Kuriki, R.; Maeda, K.; Ishitani, O.; Lau, T. C.; Bonin, J.; Robert, M. Efficient Visible-Light-Driven CO_2 Reduction by a Cobalt Molecular Catalyst Covalently Linked to Mesoporous Carbon Nitride. *J. Am. Chem. Soc.* **2020**, *142*, 6188−6195.
(29) Kuriki, R.; Sekizawa, K.; Ishitani, O.; Maeda, K. Visible-Light-Driven CO_2 Reduction with Carbon Nitride: Enhancing the Activity of Ruthenium Catalysts. *Angew. Chem.* **2015**, *127*, 2436−2439.
(30) Maeda, K.; Sekizawa, K.; Ishitani, O. A polymeric-semiconductor-metal-complex hybrid photocatalyst for visible-light CO_2 reduction. *Chem. Commun.* **2013**, *49*, 10127−10129.
(31) Lee, J.-S.; Won, D.-I.; Jung, W.-J.; Son, H.-J.; Pac, C.; Kang, S. O. Widely Controllable Syn-gas Production by a Dye-Sensitized TiO_2 Hybrid System with Re^{I} and Co^{III} Catalysts under Visible-Light Irradiation. *Angew. Chem., Int. Ed.* **2017**, *56*, 976−980.
(32) Sekizawa, K.; Sato, S.; Arai, T.; Morikawa, T. Solar-Driven Photocatalytic CO_2 Reduction in Water Utilizing a Ruthenium Complex Catalyst on *p*-Type Fe_2O_3 with a Multiheterojunction. *ACS Catal.* **2018**, *8*, 1405−1416.
(33) Kuriki, R.; Matsunaga, H.; Nakashima, T.; Wada, K.; Yamakata, A.; Ishitani, O.; Maeda, K. Nature-Inspired, Highly Durable CO_2 Reduction System Consisting of a Binuclear Ruthenium(II) Complex and an Organic Semiconductor Using Visible Light. *J. Am. Chem. Soc.* **2016**, *138*, 5159−5170.
(34) Sekizawa, K.; Maeda, K.; Domen, K.; Koike, K.; Ishitani, O. Artificial Z-Scheme Constructed with a Supramolecular Metal Complex and Semiconductor for the Photocatalytic Reduction of CO_2. *J. Am. Chem. Soc.* **2013**, *135*, 4596−4599.
(35) Wada, K.; Ranasinghe, C. S. K.; Kuriki, R.; Yamakata, A.; Ishitani, O.; Maeda, K. Interfacial Manipulation by Rutile TiO_2 Nanoparticles to Boost CO_2 Reduction into CO on a Metal-Complex/Semiconductor Hybrid Photocatalyst. *ACS Appl. Mater. Interfaces* **2017**, *9*, 23869−23877.
(36) Muraoka, K.; Uchiyama, T.; Lu, D.; Uchimoto, Y.; Ishitani, O.; Maeda, K. A Visible-Light-Driven Z-Scheme CO_2 Reduction System Using Ta_3N_5 and a Ru(II) Binuclear Complex. *Bull. Chem. Soc. Jpn.* **2019**, *92*, 124−126.
(37) Kou, Y.; Nakatani, S.; Sunagawa, G.; Tachikawa, Y.; Masui, D.; Shimada, T.; Takagi, S.; Tryk, D. A.; Nabetani, Y.; Tachibana, H.; Inoue, H. Visible light-induced reduction of carbon dioxide sensitized by a porphyrin-rhenium dyad metal complex on *p*-type semiconducting NiO as the reduction terminal end of an artificial photosynthetic system. *J. Catal.* **2014**, *310*, 57−66.
(38) Sahara, G.; Ishitani, O. Efficient Photocatalysts for CO_2 Reduction. *Inorg. Chem.* **2015**, *54*, 5096−5104.
(39) Sahara, G.; Kumagai, H.; Maeda, K.; Kaeffer, N.; Artero, V.; Higashi, M.; Abe, R.; Ishitani, O. Photoelectrochemical Reduction of CO_2 Coupled to Water Oxidation Using a Photocathode with a Ru(II)-Re(I) Complex Photocatalyst and a CoO_x/TaON Photoanode. *J. Am. Chem. Soc.* **2016**, *138*, 14152−14158.
(40) Kumagai, H.; Sahara, G.; Maeda, K.; Higashi, M.; Abe, R.; Ishitani, O. Hybrid photocathode consisting of a $CuGaO_2$ p-type semiconductor and a Ru(II)-Re(I) supramolecular photocatalyst: non-biased visible-light-driven CO_2 reduction with water oxidation. *Chem. Sci.* **2017**, *8*, 4242−4249.
(41) Ueda, Y.; Takeda, H.; Yui, T.; Koike, K.; Goto, Y.; Inagaki, S.; Ishitani, O. A Visible-Light Harvesting System for CO_2 Reduction Using a Ru^{II}-Re^{I} Photocatalyst Adsorbed in Mesoporous Organosilica. *ChemSusChem* **2015**, *8*, 439−442.
(42) Gholamkhass, B.; Mametsuka, H.; Koike, K.; Tanabe, T.; Furue, M.; Ishitani, O. Architecture of Supramolecular Metal Complexes for Photocatalytic CO_2 Reduction: Ruthenium-Rhenium Bi- and Tetranuclear Complexes. *Inorg. Chem.* **2005**, *44*, 2326−2336.
(43) Koike, K.; Naito, S.; Sato, S.; Tamaki, Y.; Ishitani, O. Architecture of supramolecular metal complexes for photocatalytic CO_2 reduction III: Effects of length of alkyl chain connecting photosensitizer to catalyst. *J. Photochem. Photobiol., A* **2009**, *207*, 109−114.
(44) Braumüller, M.; Schulz, M.; Staniszewska, M.; Sorsche, D.; Wunderlin, M.; Popp, J.; Guthmuller, J.; Dietzek, B.; Rau, S. Synthesis and characterization of ruthenium and rhenium dyes with phosphonate anchoring groups. *Dalton Trans.* **2016**, *45*, 9216−9228.
(45) Gillaizeau-Gauthier, I.; Odobel, F.; Alebbi, M.; Argazzi, R.; Costa, E.; Bignozzi, C. A.; Qu, P.; Meyer, G. J. Phosphonate-Based Bipyridine Dyes for Stable Photovoltaic Devices. *Inorg. Chem.* **2001**, *40*, 6073−6079.
(46) Tamaki, Y.; Imori, D.; Morimoto, T.; Koike, K.; Ishitani, O. High catalytic abilities of binuclear rhenium(I) complexes in the photochemical reduction of CO_2 with a ruthenium(II) photosensitiser. *Dalton Trans.* **2016**, *45*, 14668−14677.
(47) Mauzerall, D.; Westheimer, F. H. 1-Benzyldihydronicotinamide—A Model for Reduced DPN. *J. Am. Chem. Soc.* **1955**, *77*, 2261−2264.

https://dx.doi.org/10.1021/jacs.0c09170
J. Am. Chem. Soc. XXXX, XXX, XXX−XXX